Lasers in Surgery and Medicine 34:329–334 (2004)

Passive Mass Deposition Control of Cryogen Sprays Through the Use of Wire Meshes

Henry Vu, BS,[1] Guillermo Aguilar, PhD,[1,2]* and J. Stuart Nelson, MD, PhD[1]
[1]*Beckman Laser Institute, University of California, Irvine, California 92612*
[2]*Department of Mechanical Engineering, University of California, Riverside, California 92521*

Background and Objectives: Cryogen spray cooling (CSC) is used for epidermal protection during laser dermatologic surgery. However, further research is necessary to optimize the use of CSC for many applications, particularly in patients with darker skin types, and in procedures with deep-targeted chromophores.
Study Design/Materials and Methods: With the objective to enhance cryogen spray atomization and introduce a passive mass deposition control, stainless steel wire meshes of various sizes were positioned in the spray path of two nozzles of different diameters (0.7 and 1.4 mm). A temperature sensor placed at a fixed distance below the nozzle tips measured variations in temperature as a function of time. Calculations for heat flux (q), and overall heat extraction (Q) were done through an inverse heat conduction problem (IHCP) algorithm.
Results: The use of wire meshes reduced maximum q and thus cooling efficiency for both nozzles. However, for the larger diameter nozzle (1.4 mm), cooling duration was prolonged significantly when compared to the case without mesh, which led to an increase in Q.
Conclusions: Wire meshes, within the range of wire diameters used, are not desirable for use with the smaller diameter nozzle because they reduce cooling efficiency. For the larger diameter nozzle, however, the prolonged cooling duration and increase in Q may be beneficial for laser dermatological procedures directed towards deeper targeted chromophores, such as hair removal. Lasers Surg. Med. 34:329–334, 2004. © 2004 Wiley-Liss, Inc.

Key words: cryogen spray cooling; skin; port wine stain; hair removal; laser surgery; dermatology; selectivity

INTRODUCTION

Cryogen spray cooling (CSC) has become an integral part of laser dermatologic surgery, such as the treatments of port wine stain birthmarks [1], hair removal [2], and non-ablative photorejuvenation [3]. These treatments target chromophores in the dermis, but absorption of laser energy by epidermal melanin can cause excessive heating of the superficial skin layers leading to scarring or dyspigmentation [4]. The objective of CSC is to pre-cool and prevent damage to the epidermis without reducing the temperature of the deeper targeted chromophores [5].

Extensive research has been done with the objective to optimize skin cooling for each individual dermatologic procedure [2]. For example, mathematical modeling studies have shown a good compromise between spurt durations and delay times between cooling and laser pulses to maximize the effectiveness of CSC [6] for superficial targets, such as port wine stain birthmarks. A similar study [7] has also modeled skin temperature profiles induced by a contact cooling probe, which is an alternative epidermal protection procedure used during laser therapy of deeper targets, such as hair follicles. Experimental work on CSC has also been conducted to minimize the resident cryogen layer by way of multiple intermittent spurts to improve cooling efficiency [8] and, also, to determine the influence on the cooling efficiency of variables such as nozzle-to-surface distance [9], average droplet diameter and velocity [10,11].

A fundamental study of jet cooling enhancement demonstrated that the placement of perforated plates between a cooling air jet and a target surface improved heat transfer by mixing-induced turbulence [12]. In the present study, it is hypothesized that the use of fine wire meshes, with wire diameters on the same order of magnitude as the droplets, may produce similar heat transfer enhancements during CSC for the same reason. Also, it is expected that meshes may induce further droplet atomization, which increases the surface area to volume ratio, and serve as a passive mass deposition control. For this purpose, systematic measurements of heat flux (q) and overall heat extraction (Q) were carried out for two spray nozzles of different diameters, producing different spray characteristics [10], using multiple configurations in which both mesh size and placement position within the spray cone were varied.

MATERIALS AND METHODS

Cryogen Spray Formation

Two nozzles of 0.7 and 1.4 mm inner diameter (denoted narrow and wide, respectively) were used in this study.

Contract grant sponsor: National Institutes of Health (to GA and JSN); Contract grant numbers: HD-42057, GM-62177, AR-47551, AR-48458; Contract grant sponsor: Beckman Laser Institute and Medical Cline Endowment.
*Correspondence to: Guillermo Aguilar, PhD, Department of Mechanical Engineering, University of California, Riverside, CA 92521. E-mail: gaguilar@engr.ucr.edu
Accepted 19 January 2004
Published online in Wiley InterScience (www.interscience.wiley.com).
DOI 10.1002/lsm.20032

Nozzles consisted of straight stainless steel tubes welded to a copper body designed to fit an automotive fuel injector which was connected by a high-pressure hose to a commercial R-134a (1,1,1,2 tetrafluoroethane) container at saturation pressure (~6.8 bar). The fuel injector was controlled via a digital input–output channel from an SCXI-1000 chassis and PCI-6024E data acquisition card (National Instruments, Austin, TX). Spurts of user-specified durations were initiated through a custom-made Labview program. Throughout the study, spurt durations were kept uniform at 50 milliseconds with 50 milliseconds pre-purges to cool the nozzle and better simulate clinical conditions of sequential CSC/laser irradiation.

Mesh and Mesh Positioning

Type 304 stainless steel wire meshes of 150, 200, 325, and 400 mesh size (Part # 9231744 McMaster-Carr, Los Angeles, CA) (Table 1) were placed at various distances, z_m (measured from the nozzle tip to the mesh), using a BiSlide motor-driven positioning system (Velmex, Bloomfield, NY) (Fig. 1). Mean cryogen droplet diameters have been previously determined to be approximately 5 μm for the narrow nozzle and 15 μm for the wide at the spray distance of 30 mm [10] which is on the same order of magnitude as the wire diameters used. Meshes were allowed sufficient time to dry between each experiment since any water condensation and freezing on the meshes might have influenced the subsequent spurt dynamics.

Temperature Measurements

Cryogen spurts were directed onto a custom-made temperature sensor consisting of a 28 × 31 mm silver plate, 0.1 mm thick, encased on the top surface of a 7 mm thick block of epoxy resin (RBC #3100, RBC Industries, Inc. Warwick, RI). The epoxy block was used as a substrate because of its skin-like thermal properties. The thermal diffusivity for the epoxy is approximately 0.07 mm^2/second which is similar to that of human skin (0.11 mm^2/second [13]). The plate was sized to encompass the entire spray area produced by each nozzle. A type-K thermocouple of 150 μm bead diameter (5TC-TT-K-36-36 by Omega, Stanford, CT) was welded to the back surface of the silver plate and threaded out of the epoxy block. The sensor response time was estimated to be on the order of ~10 milliseconds. The sensor was placed at a fixed distance $z_s = 30$ mm below the vertically oriented nozzle which is the approximate working distance used by various commercial devices (e.g. Candela [Wayland, MA] SmoothBeam™ and GentleLASE®). The thermocouple signal was conveyed via an analog channel to the SCXI-1000 chassis and temperature data was ultimately displayed to the user through a Labview program at a sampling rate of 4 kHz.

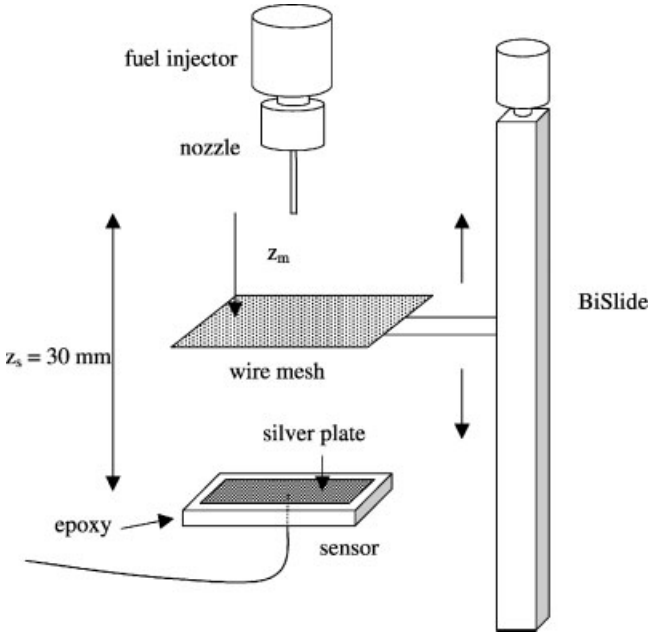

Fig. 1. Schematic of the experimental setup. The nozzle is placed at a fixed distance of $z_s = 30$ mm from the temperature sensor. Mesh position is varied vertically with the BiSlide positioning system.

To minimize inherent temperature variations in cryogen spurts, six trials for each nozzle and mesh configuration (mesh size and z_m) were carried out and the results averaged, including control measurements for each nozzle in which no mesh was used (denoted control). The sensor was allowed to warm up to ambient temperature between each experiment. The repeatability of all our experiments was excellent, as suggested by a negligible standard deviation between the six identical trials. Absolute temperature calibration of the system was not required since all analyses and comparisons were made relative to the control so all systematic errors cancelled out.

TABLE 1. Mesh Properties

Mesh size	Wire diameter (μm)	Opening width (μm)	Open area (%)
150	66	104	37.8
200	41	74	33.6
325	36	43	42.0
400	25	38	36.0

Size is based on mesh per inch or the number of openings per inch of wire mesh.

Inverse Heat Conduction Problem Algorithm

q and Q were calculated from temperature measurements through an inverse heat conduction problem (IHCP) algorithm [14]. Uniform heat transfer was assumed over the entire spray area so CSC was simplified to a one-dimensional problem represented by the following equation:

$$\rho_j c_j \frac{\partial T_j}{\partial t} = k_j \frac{\partial_j^2}{\partial y^2} \quad (1)$$

where ρ is density, c is specific heat, T is temperature, t is time, k is thermal conductivity, and subscript j denotes either the silver or epoxy layer. The epoxy was estimated

to be a semi-infinitely thick body with a diffusion time of approximately 4 minutes, so only one boundary condition at the sensor surface was required:

$$-k_{Ag}\frac{\partial T_{Ag}}{\partial y}\Big|_{y=b} = q(t) \quad (2)$$

where b is the silver plate thickness and q(t) is the estimated surface heat flux. The sequential function specification method (SFSM) [14] was used to solve the algorithm where q was calculated sequentially at each time step. Q was calculated by integration of q over time.

Video Sequence Capture

A high speed Photron Fastcam camera (Itronics, Westlake Village, CA) was used to capture video image sequences of spurts from each nozzle passing through the meshes. All images were captured at a rate of 250 frames per second. Videos were analyzed frame-by-frame and observable differences in the spray cones were noted between spurts without and with the meshes.

RESULTS

For all z_m, the measured temperatures systematically departed further from those of the control as mesh size increased from 150 to 400. Only the results for the 400 mesh are given in the following figures because this size produced the largest effect on q and Q of all meshes under study. The results for the other meshes were qualitatively similar to the 400 mesh but approached the control as mesh size decreased.

Figure 2 shows temperature measurements carried out for narrow nozzle sprays for various z_m. As z_m increased from 2.5 to 10 mm, the minimum temperatures increased by 2 to 4°C and also returned to ambient room temperature faster. This trend continued systematically as z_m increased beyond 10 mm (data not shown).

Figure 3 illustrates how q and Q are reduced in comparison to the control as z_m increases. There was a reduction in maximum q by about 3–15% and, except for $z_m = 2.5$ mm, an 11–14% reduction in maximum Q. Overall, for all z_m tested, the use of meshes appeared to reduce the maximum q and Q of the narrow nozzle, although somewhat larger q were observed at later times.

The temperature plots in Figure 4 show that for the wide nozzle, the minimum temperatures for all z_m tested compared to the control were also about 2–3°C higher, but the temperatures remained below 0°C for longer periods of time as indicated by the right shifts of the rising temperature curves. Upon examining the effect of z_m, the temperature curves tended to increase between z_m values of 2.5–10 mm but then decreased again between 10 and

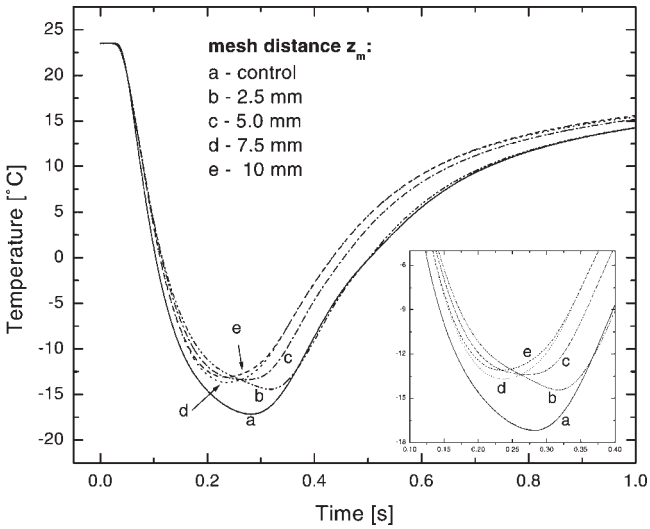

Fig. 2. Temperature plots of the narrow nozzle with the 400 mesh for various distance z_m between the nozzle tip and wire mesh.

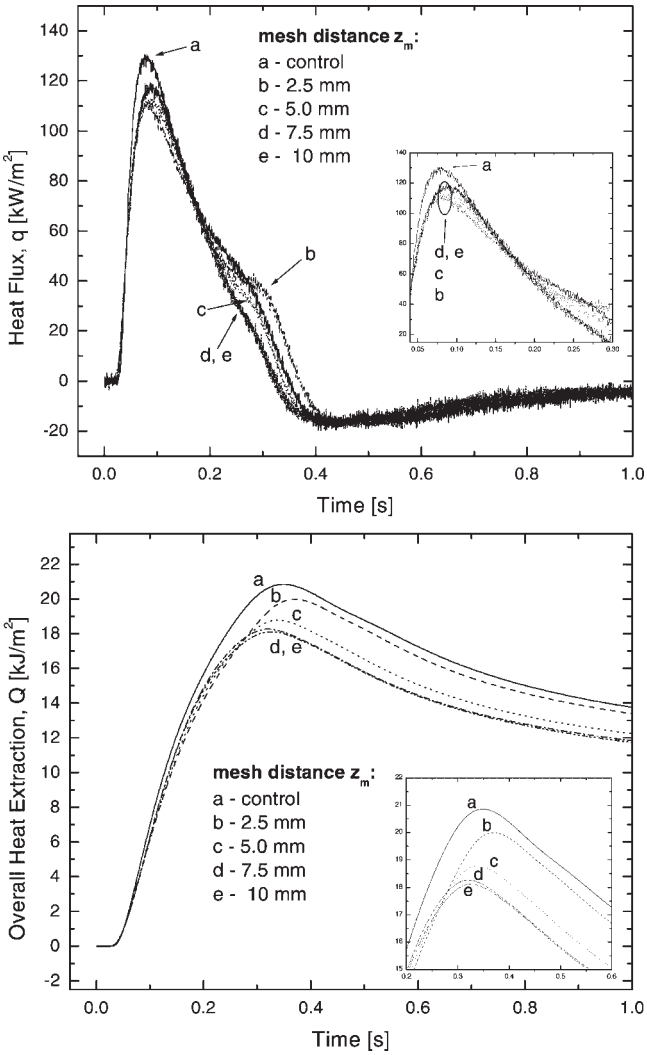

Fig. 3. Heat fluxed (q) and overall heat extractions (Q) for various z_m calculated with the 400 mesh and the narrow nozzle using the IHCP algorithm.

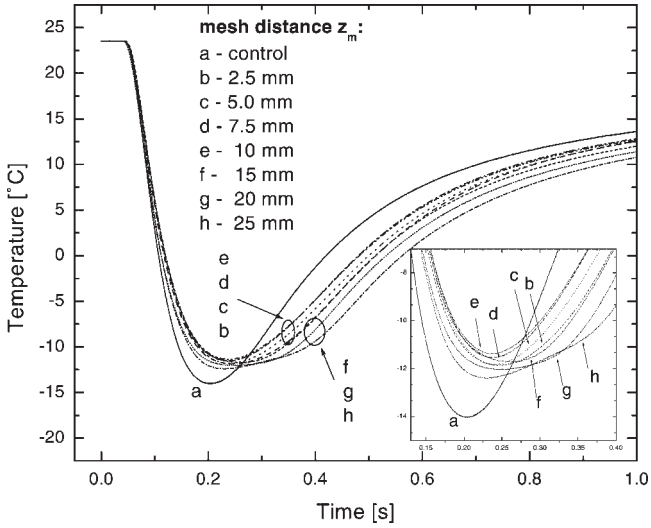

Fig. 4. Temperature plots of the wide nozzle with the 400 mesh for various z_m.

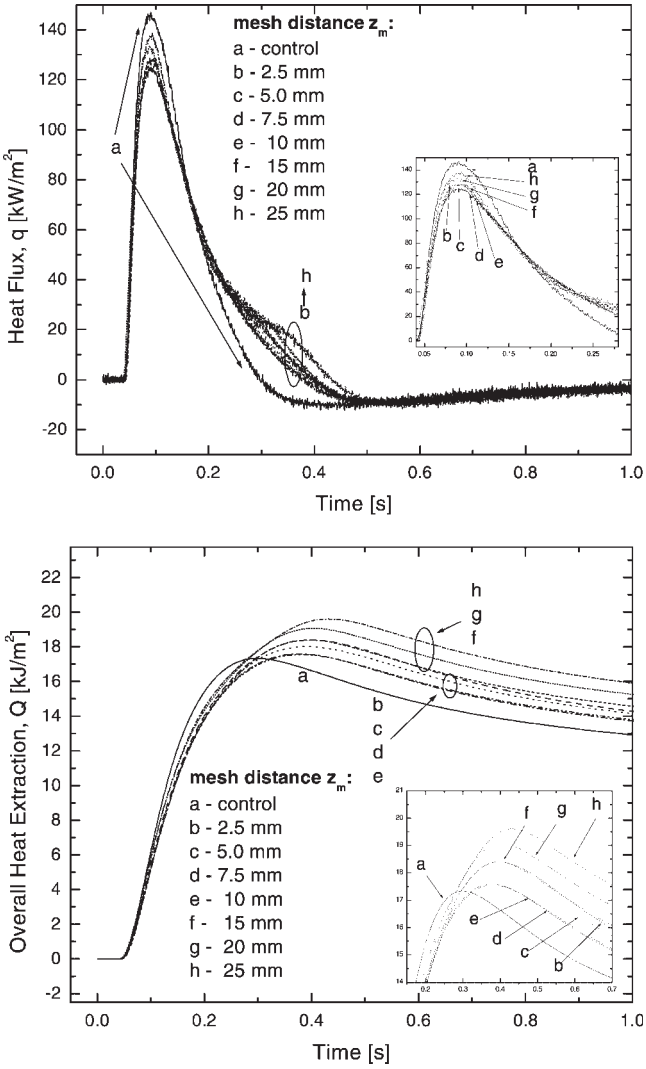

Fig. 5. q and Q calculated for the wide nozzle with the 400 mesh various z_m using the IHCP algorithm.

25 mm. Overall the sensor remained colder for longer periods of time with the finer meshes and larger z_m.

Figure 5 shows that, like the narrow nozzle, there was about a 3–15% reduction in maximum q, with somewhat larger q values at later times, but Q actually increased by a maximum of 17% at 430 milliseconds for the 400 mesh at $z_m = 25$ mm (curve h).

Selected video sequence frames are displayed in Figure 6. With the narrow nozzle, the control spurt had a wide spray cone that narrowed when wire meshes were introduced into the spray (Fig. 6a,b). Also, after the mesh, the spray appeared brighter, possibly indicating a higher reflectivity caused by more finely atomized droplets. The spray cone was narrowed further as distance z_m increased. For the wide nozzle (Figs. 6c,d), the control spurt had a straight, transparent spray. Introduction of the wire meshes did not change spray cone diameter as with the narrow nozzle. Also, an after-effect of droplets continuing to drip down from the mesh after spurt termination was observable at longer z_m.

DISCUSSION

All mesh configurations with the narrow nozzle reduced CSC efficiency (i.e., reduction in q and Q) possibly because droplets were sufficiently atomized upon release from the nozzle and their velocities were too slow [10]. Thus, upon coming into contact with the meshes, the smaller droplets evaporated and reduced the cryogen mass deposition, which, at the distance of 30 mm, may have already been close to the minimal amount necessary for optimal cooling efficiency. Average droplet temperatures may have also increased due to contact with the meshes. The observed increase in light reflectivity in the sprays with the meshes may be due to an increase in overall droplet surface area resulting from finer droplet atomization. Therefore, narrow nozzle sprays became more finely atomized with the meshes, but at the expense of significant evaporation and droplet warming.

For the wide nozzle, all mesh configurations showed prolonged cooling when compared to the control leading to enhanced Q, though the minimum temperature reached was higher and the maximum q lower. The wide nozzle spray cone was relatively transparent within the 30 mm distance used, indicating a coarse spray, possibly even an unbroken jet. As with the narrow nozzle, the observed increase in light reflectivity following the introduction of the meshes presumably was the result of increased droplet atomization. The spray cone diameter did not change significantly after the mesh, which is likely due to the higher droplet velocities and diameters [10]. The reductions in temperature fell short of the control probably because of droplet warming upon contact with the mesh.

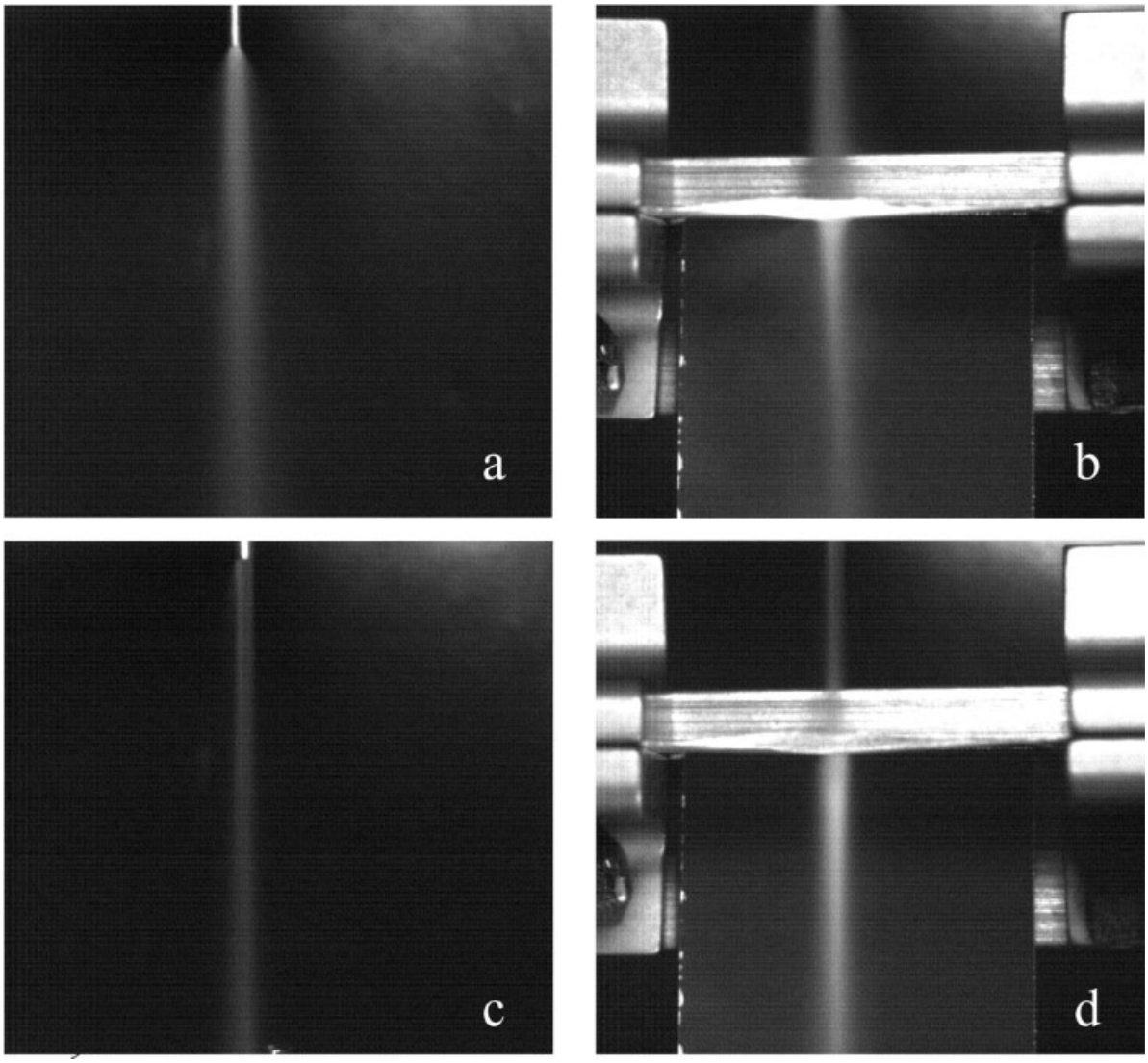

Fig. 6. Selected frames of video sequences of control cryogen spurts with 400 mesh 20 mm from the nozzle tip. **a**: control of narrow nozzle; (**b**) narrow nozzle with mesh; (**c**) control of wide nozzle; and (**d**) wide nozzle with mesh.

Evaporation of cryogen from the mesh, however, could have also limited the mass deposition on the sensor surface and, therefore, reduced the thickness of the resident cryogen layer. This would have theoretically allowed finer droplets to reach the sensor surface permitting more efficient heat extraction and thus compensate somewhat for droplet warming. The delay in maximum Q may also have been partially due to droplets dripping down from the mesh after spurt termination, which could have artificially lengthened the spurt duration slightly, as seen in Figure 5. Also, when the meshes were very close to the sensor, cooling may have been prolonged due to convection between the super-cooled mesh and the sensor. Indeed, careful observation of additional videos taken of the mesh and sensor during CSC supports this hypothesis.

Since the spurt distance $z_s = 30$ mm may not have been optimal for the wide nozzle, additional studies were performed at $z_s = 50$ and 70 mm. Figure 7 shows the calculated Q at these two longer distances z_s using the 400 mesh at $z_m = 45$ and 65 mm, respectively (i.e., in all cases $z_s - z_m = 5$ mm). These curves are compared to the highest Q obtained at $z_s = 30$ mm and to the control for the narrow nozzle also at $z_s = 30$ mm (standard clinical). Highest Q was obtained with $z_s = 50$ mm. However, this value of Q was only marginally higher than the control with the narrow nozzle, but it occurred at a much later time. Therefore, this particular configuration of the wide nozzle, $z_s = 50$ mm, $z_m = 45$ mm, and 400 mesh size would allow for larger heat extraction from deeper targets for the same nozzle/valve, position, and spurt duration configuration.

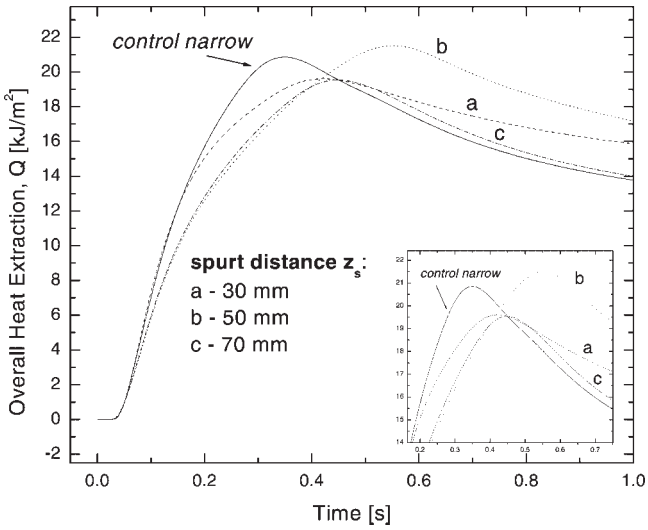

Fig. 7. Calculated Q for various z_s using the wide nozzle in comparison to control for narrow nozzle.

Another important point to note is that though the wire diameters of the mesh sizes used (25–66 μm) were on the same order of magnitude as the droplet diameters at the spray distance of $z_s = 30$ mm (5–15 μm), they were still larger. Using mesh sizes with smaller wire diameters may increase droplet atomization and produce different results.

CONCLUSION

All meshes used with the narrow nozzle showed reduced CSC efficiency compared to the control. The meshes used are thus undesirable for use with nozzle geometries similar to the narrow nozzle (e.g., commercial nozzles). However, with the wide nozzle, the prolonged cooling and delay in maximum Q when meshes were used may be beneficial in laser therapies aimed at deeper targets, such as hair removal, where longer but less intense cooling is preferred.

Some cryogen evaporates upon contact with the relatively warm meshes, so droplet temperatures may increase while reducing the cryogen mass deposited on the target. These effects along with an increase in droplet atomization would reduce cooling efficiency but prolong the cooling time and, thus, allow larger heat extraction from deeper targets. Cooling can also be prolonged after spurt termination due to droplets dripping down from the mesh and from convective heat transfer between the mesh and target surface. In clinical practice, it would be necessary to delay the subsequent laser pulse until after the maximum Q has been reached to achieve the maximum cooling benefits. Technical difficulties may arise, however, from mesh placement and from frost formation on the mesh, which could block subsequent spurts.

Finally, spurt duration, spurt distance, and the range of mesh sizes used in this study may not be optimal. Short spurt durations seem to lead to excessive droplet evaporation upon contact with the mesh, while long ones appear to enhance frost formation, inhibiting incoming droplets from reaching the targeted surface and prolonging the heat extraction with lower CSC efficiency. Further research may help determine the appropriate choice of these parameters to meet the requirements of cooling selectivity of various applications.

ACKNOWLEDGMENTS

Laboratory assistance and data analysis provided by Brooke Basinger, Daniel Evans, and Jie Liu are greatly appreciated.

REFERENCES

1. Nelson JS, Milner TE, Anvari B, Tanenbaum BS, Kimel S, Svaasand LO, Jacques SL. Dynamic epidermal cooling during pulsed laser treatment of port-wine stain. A new methodology with preliminary clinical evaluation. Arch Dermatol 1995;131(6):695–700.
2. Nelson JS, Majaron B, Kelly KM. Active skin cooling in conjunction with laser dermatologic surgery. Semin Cutan Med Surg 2000;19(4):253–266
3. Nelson JS, Majaron B, Kelly KM. What is nonablative photorejuvenation of human skin? Semin Cutan Med Surg 2002;21(4):238–250.
4. Chang CJ, Nelson JS. Cryogen spray cooling and higher fluence pulsed dye laser treatment improve port-wine stain clearance while minimizing epidermal damage. Dermatol Surg 1999;25:767–772.
5. Nelson JS, Milner TE, Anvari B , Tanenbaum BS, Svaasand LO, Kimel S. Dynamic epidermal cooling in conjunction with laser-induced photothermolysis of port wine stain blood vessels. Lasers Surg Med 1996;19(2):224–229.
6. Verkruysse W, Majaron B, Tanenbaum BS, Nelson JS. Optimal cryogen spray cooling parameters for pulsed laser treatment of port wine stains. Lasers Surg Med 2000;27(2): 165–170.
7. Altshuler GB, Zenzie HH, Erofeev AV, Smirnov MZ, Anderson RR, Dierickx C. Contact cooling of the skin. Phys Med Biol 1999;19(2):224–229.
8. Majaron B, Svaasand LO, Aguilar G, Nelson JS. Intermittent cryogen spray cooling for optimal heat extraction during dermatologic laser treatment. Phys Med Biol 2002;47(18): 3275–3288.
9. Aguilar G, Majaron B, Pope K, Svaasand LO, Lavernia EJ, Nelson JS. Influence of nozzle-to-skin distance in cryogen spray cooling for dermatologic laser surgery. Lasers Surg Med 2001;28(2):113–120.
10. Aguilar G, Majaron B, Karapetian E, Lavernia EJ, Nelson JS. Experimental study of cryogen spray properties for application in dermatologic laser surgery. IEEE Trans Biomed Eng 2003;50(7):863–869.
11. Pikkula BM, Torres JH, Tunnell JW, Anvari B. Cryogen spray cooling: Effects of droplet size and spray density on heat removal. Lasers Surg Med 2001;28(2):103–112.
12. Lee DH, Young ML, Kim YT, Won SY, Chung YS. Heat transfer enhancement by the perforated plate installed between an impinging jet and the target plate. Int J Heat Mass Transfer 2002;45:213–217.
13. Duck FA. Physical properties of tissue: A comprehensive reference book. London: Academic Press; 1990.
14. Beck JV, Blackwell B, St Clair CR. Inverse heat conduction: Ill-posed problems. New York: Wiley; 1985.